Journal of Solid State Chemistry 181 (2008) 3131–3136

Contents lists available at ScienceDirect

Journal of Solid State Chemistry

journal homepage: www.elsevier.com/locate/jssc

Polar domains and charge-density waves in the acentric cerium(III) iron(II) sulfide $Ce_{22}Fe_{21}S_{54}$

Allison M. Mills, Michael Ruck *

Department of Chemistry and Food Chemistry, Dresden University of Technology, D-01062 Dresden, Germany

ARTICLE INFO

Article history:
Received 24 April 2008
Received in revised form
21 July 2008
Accepted 3 August 2008
Available online 19 August 2008

Keywords:
Cerium
Charge-density wave
Domain walls
Iron
Multiferroic materials
Polar crystal structure

ABSTRACT

The cerium(III) iron(II) sulfide $Ce_{22}Fe_{21}S_{54}$ was synthesized through reaction of the binary sulfides *C*-Ce_2S_3 and FeS in a LiCl/KCl flux at 1170 K, and its structure was determined by single-crystal X-ray diffraction. $Ce_{22}Fe_{21}S_{54}$ crystallizes in the polar monoclinic space group *Cm* with $a = 16.3912(7)$ Å, $b = 3.9554(1)$ Å, $c = 62.028(3)$ Å, $\beta = 94.831(4)^\circ$, and $Z = 2$. The structure is a superstructure of the $La_2Fe_2S_5$ structure type. Akin to the parent structure, *trans*-edge-sharing [FeS_6]-octahedra form linear chains, which are isotactically capped on one side by [FeS_4]-tetrahedra. The polarity of the resulting $^1_\infty$[Fe_2S_5]-chains is transferred to the entire structure, as the unit cell contains two layered domains of opposite polarity with the unbalanced size ratio of 4:6. The domain walls are intrinsically centrosymmetric (layer group *c* 1 2/*m* 1). One wall consists of trigonal [FeS_5]-bipyramids, which are linked by corners and edges into a $^2_\infty$[Fe_2S_5]-layer. In the other wall, the [FeS_4]-tetrahedra of two opposing $^1_\infty$[Fe_2S_5]-chains share their vertices. The sulfur anions eliminated thereby are counterbalanced by vacancies in the iron sites, which follow a sinusoidal occupation modulation corresponding to a frozen charge-density wave with the wave vector $k = 4\pi c^*\cdot$ The coordination polyhedra of all the cerium cations are bicapped trigonal prisms.

1. Introduction

Compounds in the ternary *Ln*–*T*–S systems (*Ln* = lanthanoid, *T* = transition metal) are of interest because of their potential for interesting physical properties [1]. For example, the unprecedented observation of mobile Ln^{3+} cations in $La_{52}Fe_{12}S_{90}$ [2] and in the related sulfide halogenides $Ln_{53}Fe_{12}S_{90}X_3$ (*Ln* = La, Ce; *X* = Cl, Br, I) [3] was recently reported. In the context of the current search for multiferroic materials [4], the sulfosalts $Ln_2Fe_2S_5$ [5,6] and $Ln_3Fe_2S_7$ (*Ln* = La, Ce) [7] arouse special interest. The crystal structures of these magnetically ordering semiconductors [8] include polar axes, which allow for ferro-, piezo- and pyroelectricity.

The $La_2Fe_2S_5$ structure type is rather unusual, since it contains Fe^{2+} cations in both octahedral and tetrahedral sites (Fig. 1). The [FeS_6]-octahedra share *trans*-edges to form linear chains, and the [FeS_4]-tetrahedra bridge pairs of octahedra within these chains by sharing edges with them. The resulting $^1_\infty$[Fe_2S_5]-chains run along the [100] direction, with all of the [FeS_4]-tetrahedra on the same side. Thus, the structure is polar and one-dimensional in character. Typically, vacancies occur in the octahedral iron sites, leading to nonstoichiometric compounds $Ln_2Fe_{2-\delta}S_5$. The presence of vacancies entails the oxidation of some Fe^{2+} cations to Fe^{3+} in order to compensate the charge [6].

Herein, we report on the hitherto unknown cerium(III) iron(II) sulfide $Ce_{22}Fe_{21}S_{54}$. Its complex crystal structure is based on well-defined domains of the $Ce_2Fe_2S_5$ structure, which alternate periodically, but asymmetrically, in their polarity.

2. Experimental

2.1. Synthesis and chemical analysis

Silver-colored, air-insensitive crystals of the compound $Ce_{22}Fe_{21}S_{54}$ were unexpectedly obtained from a reaction designed to produce the stoichiometric compound $Ce_2Fe_2S_5$. Starting reactants were the binary sulfides *C*-Ce_2S_3 and FeS. *C*-Ce_2S_3 was synthesized by heating stoichiometric amounts of cerium (rod, > 99.5%, Treibacher; freshly filed under argon prior to use) and sulfur (powder, > 99%, VEB Laborchemie; recrystallized from CS_2, and then purified of carbon according to the method of *von Wartenberg* [9]) at 1370 K. FeS was prepared by heating stoichiometric amounts of iron (powder, 99.9%, ABCR; treated with H_2 at 770 K) and sulfur at 1170 K. An equimolar mixture of LiCl (p.a., Merck) and KCl (p.a., J. T. Baker), which was first heated

* Corresponding author. Fax: +49 351 463 37287.
E-mail address: Michael.Ruck@chemie.tu-dresden.de (M. Ruck).

0022-4596/$ - see front matter © 2008 Elsevier Inc. All rights reserved.
doi:10.1016/j.jssc.2008.08.011

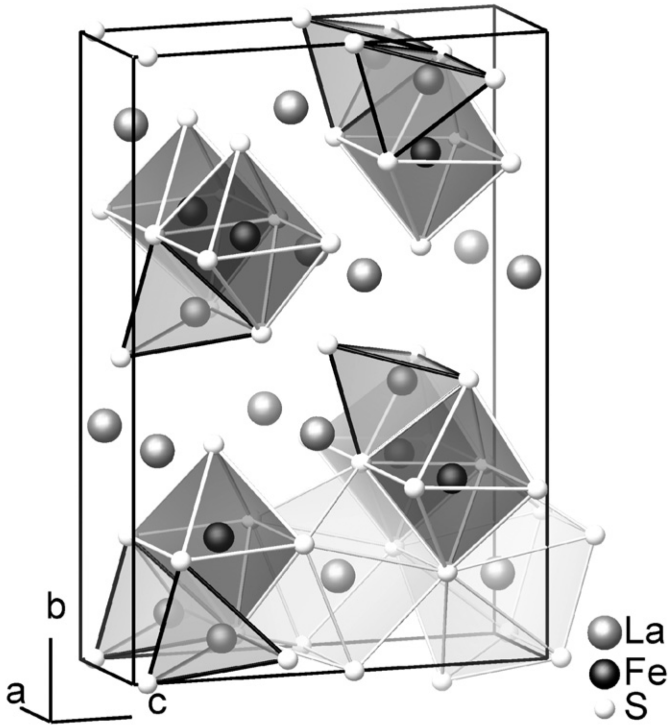

Fig. 1. The polar crystal structure of $La_2Fe_2S_5$ with Fe^{2+} cations in octahedra and tetrahedra, and La^{3+} cations in bicapped trigonal prisms.

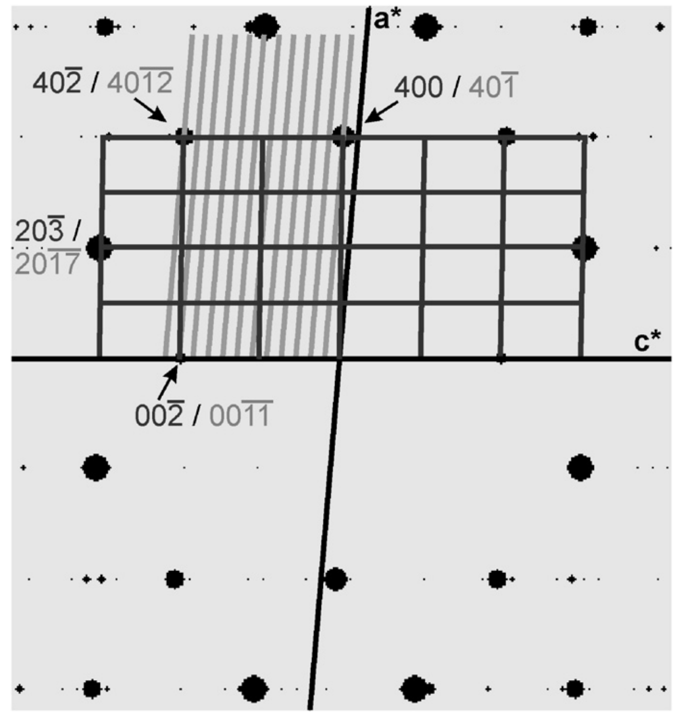

Fig. 2. Schematic representation of the $h0l$ diffraction pattern of $Ce_{22}Fe_{21}S_{54}$ [15]. The light gray lines correspond to the monoclinic cell with $c \approx 62$ Å; the black grid represents the pseudo-orthorhombic subcell with $c' \approx 11.3$ Å.

Table 1
Crystallographic data and details of the structure determination for $Ce_{22}Fe_{21}S_{54}$

Formula	$Ce_{22}Fe_{21}S_{54}$
Crystal system, space group	Monoclinic, *Cm* (No. 8)
Cell parameters	$a = 16.3912(7)$ Å, $b = 3.9554(1)$ Å, $c = 62.028(3)$ Å $\beta = 94.831(4)^\circ$, $V = 4007.2(3)$ Å^3
Formula units per cell	$Z = 2$
Calculated density	$\rho_{calc} = 4.96\,g\,cm^{-1}$
Crystal dimensions	0.07 mm × 0.04 mm × 0.01 mm
Temperature	293(1) K
Measurement device	Imaging-plate diffractometer (Stoe IPDS-II)
Radiation	Graphite-monochromated Mo*K*α ($\lambda = 0.71073$ Å)
Measurement limits	$2.6^\circ \leqslant 2\theta \leqslant 54.4^\circ$ $-20 \leqslant h \leqslant 20, -4 \leqslant k \leqslant 5, -79 \leqslant l \leqslant 77$
Scan type	$0 \leqslant \omega \leqslant 180^\circ$, $\Delta\omega = 0.5^\circ$; $\phi_1 = 60$, $\phi_2 = 95^\circ$
Absorption correction	Numerical, on the basis of a crystal description optimized using equivalent reflections [10,11]
Absorption coefficient	$\mu(MoK\alpha) = 173\,cm^{-1}$
Transmission factors	0.33–0.87
Number of reflections	21718 measured, 8339 independent
Data averaging	$R_{int} = 0.066$, $R_\sigma = 0.060$
Structure refinement	Full-matrix least-squares on F_o^2 [12]; anisotropic displacement parameters; inversion twin with domain ratio of 0.37(5):0.63(5)
Extinction parameter	$9.1(5) \times 10^{-5}$
Number of parameters, restraints	597, 3
Residual electron density	+1.94 to –1.86 e Å^{-3}
Figures of merit	R_1 (all F_o) = 0.075 R_1 (5334 $F_o > 4\sigma(F_o)$) = 0.045 wR_2 (all F_o) = 0.097
Goodness of fit	1.18

under dynamic vacuum to remove any moisture, was used as a flux. The sulfides *C*-Ce_2S_3 and FeS, in a ratio of 1:2 (0.25 g in total), were combined with the LiCl/KCl flux (0.5 g) in a fused silica ampoule (12-cm length, 1.5-cm diameter), which was then sealed

Table 2
Coordinates and equivalent isotropic displacement parameters (in pm^2) for $Ce_{22}Fe_{21}S_{54}$

Atom	*X*	*Z*	U_{eq}
Ce1	0.0084(2)	0.03716(6)	189(7)
Ce2	0.7672(2)	0.05614(6)	236(8)
Ce3	0.7793(2)	0.12727(6)	203(7)
Ce4	0.0337(2)	0.14829(6)	197(7)
Ce5	0.0680(2)	0.21885(6)	217(8)
Ce6	0.8266(2)	0.23994(6)	207(7)
Ce7	0.8372(2)	0.31065(6)	219(8)
Ce8	0.0921(2)	0.33103(6)	206(8)
Ce9	0.1106(2)	0.39954(6)	247(8)
Ce10	0.8702(2)	0.42380(6)	188(7)
Ce11	0.8719(2)	0.49352(7)	267(9)
Ce12	0.1293(2)	0.51113(7)	291(9)
Ce13	0.1296(2)	0.58023(6)	230(8)
Ce14	0.8915(2)	0.60467(7)	268(8)
Ce15	0.9066(2)	0.67278(6)	202(8)
Ce16	0.1611(2)	0.69328(6)	209(8)
Ce17	0.1715(2)	0.76402(6)	186(7)
Ce18	0.9299(2)	0.78495(5)	189(7)
Ce19	0.9642(2)	0.85561(6)	195(7)
Ce20	0.2194(2)	0.87690(6)	194(7)
Ce21	0.2323(2)	0.94795(6)	191(7)
Ce22	0.9910(2)	0.96677(6)	212(7)
Fe1	0.6688(9)	0.0005(2)	940(40)
Fe2	0.3368(5)	0.0039(2)	290(20)
Fe3	0.1019(5)	0.0898(2)	480(40)
Fe4	0.4610(5)	0.0984(2)	390(20)
Fe5	0.7238(5)	0.1800(2)	380(20)
Fe6	0.3654(5)	0.1906(2)	260(20)
Fe7	0.1564(5)	0.2719(2)	380(30)
Fe8	0.5179(5)	0.2827(1)	410(20)
Fe9	0.7763(6)	0.3644(2)	350(30)
Fe10	0.4057(4)	0.3737(2)	270(20)
Fe11	0.1922(7)	0.4540(2)	310(40)
Fe12	0.5361(4)	0.4652(1)	600(20)
Fe13	0.8029(7)	0.5485(2)	300(40)
Fe14	0.4242(2)	0.5548(1)	380(10)

Table 2 (*continued*)

Atom	X	Z	U_{eq}
Fe15	0.2189(5)	0.6395(2)	330(20)
Fe16	0.5911(6)	0.6307(2)	520(30)
Fe17	0.8396(4)	0.7320(2)	230(20)
Fe18	0.4740(3)	0.7216(1)	260(20)
Fe19	0.2747(4)	0.8235(2)	220(20)
Fe20	0.6343(5)	0.8133(2)	300(20)
Fe21	0.8984(4)	0.9150(1)	190(20)
Fe22	0.5312(4)	0.9047(1)	230(20)
S1	0.504(1)	0.0020(3)	240(10)
S2	0.1824(7)	0.0222(3)	230(30)
S3	0.3754(7)	0.0402(2)	220(30)
S4	0.5939(7)	0.0624(2)	200(30)
S5	0.9421(8)	0.0806(2)	220(30)
S6	0.2504(7)	0.0899(2)	210(30)
S7	0.5995(7)	0.1180(3)	200(30)
S8	0.4087(7)	0.1318(2)	170(30)
S9	0.2106(8)	0.1545(2)	190(30)
S10	0.8757(7)	0.1725(3)	250(30)
S11	0.5750(8)	0.1825(2)	200(30)
S12	0.2428(8)	0.2084(3)	230(30)
S13	0.4373(8)	0.2235(3)	220(30)
S14	0.6546(8)	0.2459(3)	250(30)
S15	−0.0010(8)	0.2639(2)	220(30)
S16	0.3063(7)	0.2746(2)	160(30)
S17	0.6576(8)	0.3008(2)	270(40)
S18	0.4665(8)	0.3155(2)	290(30)
S19	0.2697(8)	0.3384(3)	210(30)
S20	0.9354(9)	0.3573(3)	310(30)
S21	0.6316(8)	0.3646(2)	220(30)
S22	0.2904(8)	0.3934(2)	230(30)
S23	0.4861(8)	0.4078(3)	270(40)
S24	0.6921(7)	0.4274(3)	250(30)
S25	0.0399(4)	0.4478(2)	280(20)
S26	0.351(1)	0.4577(3)	290(30)
S27	0.6946(8)	0.4823(3)	250(30)
S28	0.497(1)	0.5015(4)	270(10)
S29	0.3085(8)	0.5212(3)	210(30)
S30	0.9795(5)	0.5440(2)	330(20)
S31	0.654(1)	0.5466(2)	280(30)
S32	0.3089(8)	0.5759(3)	240(30)
S33	0.5145(9)	0.5945(3)	340(40)
S34	0.7105(8)	0.6107(3)	220(30)
S35	0.3736(7)	0.6381(3)	250(30)
S36	0.052(1)	0.6432(3)	510(50)
S37	0.7268(8)	0.6662(3)	280(40)
S38	0.5289(6)	0.6869(2)	170(30)
S39	0.3427(7)	0.7027(2)	200(30)
S40	0.6873(8)	0.7293(3)	280(40)
S41	0.9994(7)	0.7376(3)	270(30)
S42	0.3441(7)	0.7581(2)	160(30)
S43	0.5557(8)	0.7790(3)	200(30)
S44	0.7558(7)	0.7939(2)	200(30)
S45	0.4249(7)	0.8207(2)	230(30)
S46	0.1194(8)	0.8306(3)	220(30)
S47	0.7879(8)	0.8503(3)	220(30)
S48	0.5853(7)	0.8713(3)	220(30)
S49	0.4017(7)	0.8869(2)	230(30)
S50	0.7468(8)	0.9120(2)	210(30)
S51	0.0610(8)	0.9220(3)	250(30)
S52	0.3981(7)	0.9411(3)	220(30)
S53	0.6222(8)	0.9637(2)	220(30)
S54	0.8161(9)	0.9814(3)	270(30)

All atoms lie on the mirror plane at $y = 0$. Partially occupied sites: Fe2 (81(1)%), Fe3 (96(4)%), Fe9 (81(1)%), Fe11 (68(2)%), Fe13 (78(4)%), Fe21 (96(2)%).

under vacuum (10^{-3} Torr). The reaction mixture was heated at 1170 K for 6 days, and then cooled to room temperature at a rate of 100 K h^{-1}. The flux was removed by washing the sample several times with water and then ethanol. The product contained platelets of $Ce_{22}Fe_{21}S_{54}$ as the majority phase, small needles of $Ce_2Fe_{2-\delta}S_5$ (about 20%) and some micro-crystalline powder of Fe_xS impurity phases. The energy-dispersive X-ray (EDX) analyses of a $Ce_{22}Fe_{21}S_{54}$ single crystal (previously identified by X-ray precession photographs) on a CamScan CS44 scanning electron microscope resulted in: Ce 24.1(4), Fe 17.7(9), S 58(1) mol% (average of three analyses).

2.2. X-ray structure determination

Intensity data for a single crystal of $Ce_{22}Fe_{21}S_{54}$ were collected at 293 K using graphite-monochromated Mo*K*α radiation, on a Stoe IPDS-II diffractometer. Crystal data and further details of the data collection are given in Table 1.

The strong reflections in the diffraction images (Fig. 2) could be indexed according to a monoclinic—almost orthorhombic—*C*-centered cell ($a' \approx 16.4$ Å, $b' \approx 3.95$ Å, $c' \approx 11.3$ Å, $\beta' \approx 90^\circ$), which resembles the orthorhombic cell of $La_2Fe_2S_5$ (space group $Cmc2_1$, $a = 3.997(2)$ Å, $b = 16.485(5)$ Å, $c = 11.394(4)$ Å [5]). However, numerous additional weak reflections along the c^* direction lead to an enlarged *c*-axis of about $11c'/2 \approx 62$ Å and a monoclinic angle of $\beta \approx 95^\circ$.

A numerical absorption correction was applied with the program X-RED [10] based on a crystal description optimized

Table 3
Survey of interatomic distances (in pm) for $Ce_{22}Fe_{21}S_{54}$. Ce–S distances are listed up to 346 pm (next: 372 pm) and Fe–S distances up to 303 pm (next: 324 pm)

Ce1–S	btp	282–307(1)
Ce2–S	btp	289–313(1)
Ce3–S	btp	289–310(1)
Ce4–S	btp	289–310(1)
Ce5–S	btp	289–310(1)
Ce6–S	btp	287–308(1)
Ce7–S	btp	290–319(1)
Ce8–S	btp	290–315(1)
Ce9–S	btp	288–330(1)
Ce10–S	btp	292–304(1)
Ce11–S	btp	286–346(1)
Ce12–S	btp	293–332(1)
Ce13–S	btp	292–319(1)
Ce14–S	btp	290–340(1)
Ce15–S	btp	290–313(2)
Ce16–S	btp	286–346(1)
Ce17–S	btp	288–314(1)
Ce18–S	btp	287–324(1)
Ce19–S	btp	288–309(1)
Ce20–S	btp	286–318(2)
Ce21–S	btp	279–311(1)
Ce22–S	btp	289–309(2)
Fe1–S	tbp	234–278(2)
Fe2–S	tbp	229–286(2)
Fe3–S	oct	243–264(2)
Fe4–S	tet	227–248(2)
Fe5–S	oct	246–265(1)
Fe6–S	tet	227–237(2)
Fe7–S	oct	245–267(2)
Fe8–S	tet	227–246(2)
Fe9–S	oct	237–268(2)
Fe10–S	tbp	230–299(2)
Fe11–S	oct	249–265(2)
Fe12–S	tbp	226–303(2)
Fe13–S	oct	243–293(2)
Fe14–S	tbp	230–277(2)
Fe15–S	oct	254–277(2)
Fe16–S	tbp	224–299(2)
Fe17–S	oct	249–269(2)
Fe18–S	tet	224–240(1)
Fe19–S	oct	248–270(1)
Fe20–S	tet	227–241(2)
Fe21–S	oct	248–266(2)
Fe22–S	tet	228–232(2)

The highest estimated standard deviation of a single distance is given in brackets. Coordination polyhedra: bicapped trigonal prism (btp), trigonal bipyramid (tbp), octahedron (oct), tetrahedron (tet).

using equivalent reflections with X-SHAPE [11]. The structure was solved in the acentric space group *Cm* by direct methods using SHELXS97, and refined on F^2 using SHELXL97 [12]. After all cerium, sulfur, and iron atoms had been located through repeated refinements and difference Fourier syntheses, the occupancies of the iron sites were checked. Significant vacancies were found on the Fe2, Fe3, Fe9, Fe11, Fe13, and Fe21 positions, leading to the approximate sum formula $Ce_{22}Fe_{21}S_{54}$, which is consistent with the EDX analyses.

In subsequent refinements, the sum of occupancies of these iron positions was constrained to assure electroneutrality. All atoms were refined with anisotropic displacement parameters. The crystal was an unbalanced inversion twin, the relative fractional contributions of the twin components being 0.37(5):0.63. Final values of the positional and displacement parameters are given in Table 2. Selected interatomic distances are listed in Table 3. The estimated standard deviations of the refined parameters might be somewhat unrealistic, owing to large correlations between parameter shifts due to the translational pseudosymmetry. In addition, the vacancies on the iron positions give rise to disorder phenomena, which influence the displacement parameters.

Further data, in the form of a CIF, have been deposited with the Fachinformationszentrum Karlsruhe, D-76344 Eggenstein-Leopoldshafen, Germany (E-mail address: crysdata@fiz-karlsruhe.de), as supplementary material No. CSD 419390, and can be obtained by contacting the FIZ (quoting the article details and the corresponding CSD number). Graphics were prepared using the program DIAMOND [13].

3. Results and discussion

Crystals of the cerium(III) iron(II) sulfide $Ce_{22}Fe_{21}S_{54}$ were obtained through reaction of the binary sulfides C-Ce_2S_3 and FeS in a LiCl/KCl flux at 1170 K. The light gray, shiny platelets are insensitive to air and moisture. The assignment of the oxidation state Ce^{III} for $Ce_{22}Fe_{21}S_{54}$ was made in accordance with that verified by analysis of the X-ray absorption near-edge structure (XANES) of the Ce $M_{IV,V}$ edge for the chemically, as well as structurally, related compound $Ce_2Fe_{1.82}S_5$ [6]. Since the samples containing $Ce_{22}Fe_{21}S_{54}$ were not phase-pure neither Moessbauer spectroscopy nor magnetic measurements could be used for further investigations on the oxidation states.

X-ray diffraction on a single crystal at 293(1) K showed that $Ce_{22}Fe_{21}S_{54}$ crystallizes in the polar monoclinic space group *Cm* with lattice parameters $a = 16.3912(7)$ Å, $b = 3.9554(1)$ Å, $c = 62.028(3)$ Å, and $\beta = 94.831(4)^\circ$. The cell contains two formula units, i.e. 194 atoms, of which 98 are symmetry-independent. All atoms lie on the mirror planes at $y = 0$ or $y = 1/2$ (Fig. 3). The crystal structure of $Ce_{22}Fe_{21}S_{54}$ has substantial similarity to the orthorhombic $La_2Fe_2S_5$ structure type (space group $Cmc2_1$, $a = 3.997(2)$ Å, $b = 16.485(5)$ Å, $c = 11.394(4)$ Å [5]). While the dimensions of the (a,b)-planes are almost the same in both structures, the c-axis is 5.5 times longer in the structure of $Ce_{22}Fe_{21}S_{54}$. Akin to the parent structure, $[FeS_6]$-octahedra share *trans*-edges to form linear $^1_\infty[Fe_{oct}S_2S_{4/2}]$-chains (octahedral chains) that run along the [010] direction. $[FeS_4]$-tetrahedra bridge pairs of octahedra on the same side of the chains, by each sharing two edges with two octahedra and two vertices with each other. The resulting chains have the composition $^1_\infty[(Fe_{oct}SS_{2/2}S_{3/3})(Fe_{tet}SS_{3/3})] = ^1_\infty[Fe_2S_5]$. Parallel to the (a,b)-plane, $^1_\infty[Fe_2S_5]$-chains of the same orientation are arranged into $^2_\infty[Fe_2S_5]$-layers, which are connected by the cerium atoms. All the cerium atoms are eight-coordinate, with a similar bicapped trigonal prismatic coordination environment of sulfur atoms. Such capped rare-earth-centered trigonal prisms are commonly observed in ternary rare-earth sulfides.

The isotactic capping octahedral chains by $[FeS_4]$-tetrahedra induces structural polarity, which is not compensated by a center

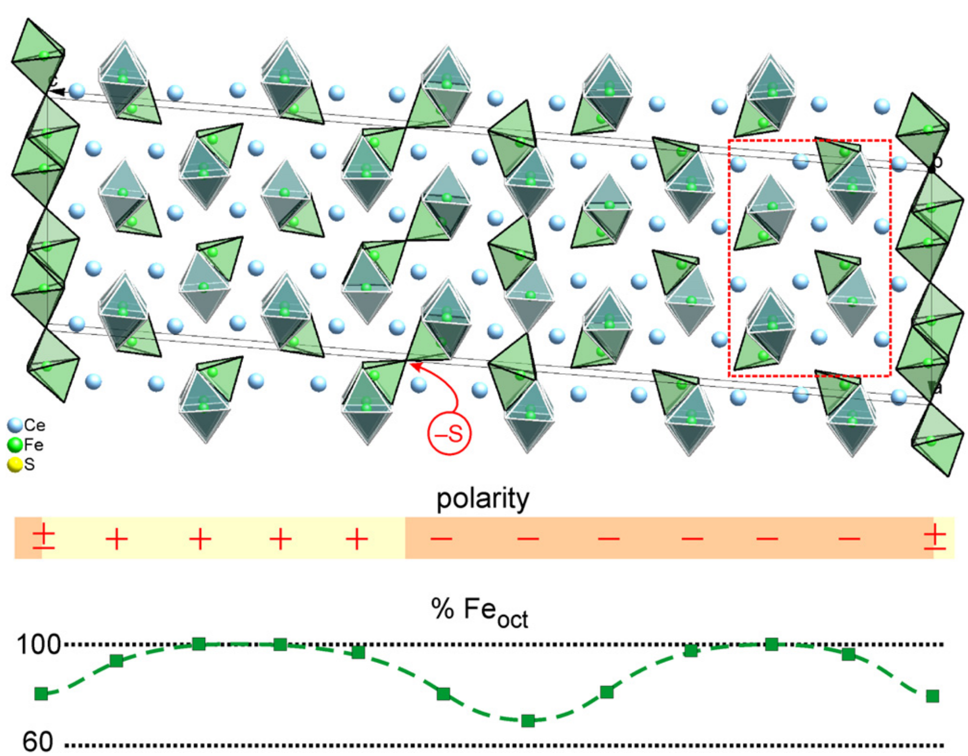

Fig. 3. View down the [010] direction of the crystal structure of $Ce_{22}Fe_{21}S_{54}$ highlighting the iron-centered $[FeS_n]$-polyhedra. All atoms reside on mirror planes at $y = 0$ or $y = 1/2$. The subcell of the $La_2Fe_2S_5$ structure type is indicated with broken outline. Below, the polarity induced by the isotactic capping of the chains of $[FeS_6]$-octahedra as well as the occupancies of the octahedral iron sites (including those in the tbp domain wall) are denoted.

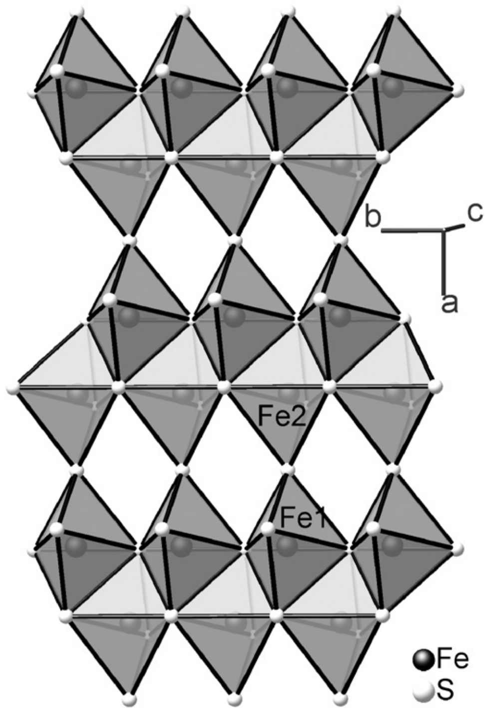

Fig. 4. Domain wall of $[FeS_5]$-trigonal bipyramids at $z \approx 0$ in $Ce_{22}Fe_{21}S_{54}$.

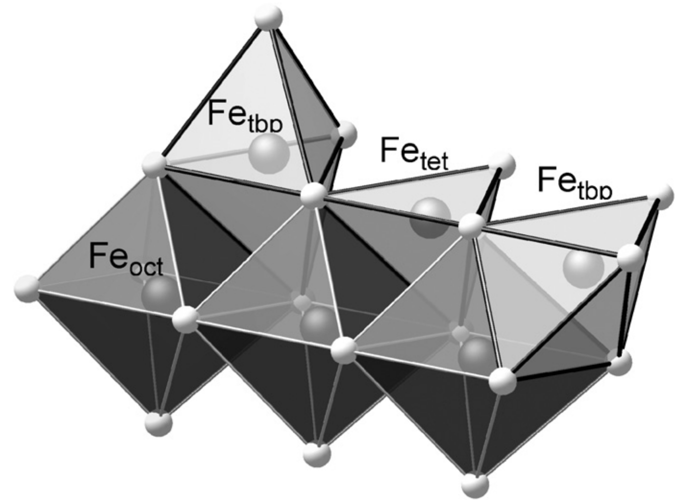

Fig. 5. Section of a $^1_\infty[Fe_2S_5]$-chain showing the tetrahedral and the two trigonal-bipyramidal coordination modes.

of inversion. In the unit cell, there are two domains with opposite polarities but—and this is essential—different widths. Referring to the representation in Fig. 3, one domain comprises *four* $^2_\infty[Fe_2S_5]$-layers with their tetrahedra pointing to the right (sign "+"), while the other domain consists of *six* $^2_\infty[Fe_2S_5]$-layers with their tetrahedra pointing to the left (sign "–"). In consequence, the compound is polar, although opposite orientations of the $^1_\infty[Fe_2S_5]$-chains occur in the unit cell. Furthermore, the structure determination indicated an unbalanced inversion twin with a volume ratio of 0.37(5):0.63(5), which also does not eliminate the polarity of the crystal. The fact that the calculated inversion-twin volume ratio is equal to the domain size ratio in the unit cell is almost certainly an artifact of the calculation.

The two layered domains of opposite polarity face each other at two types of domain walls, which are intrinsically centrosymmetric (layer group *c* 1 2/*m* 1). The wall at $z \approx 0$ consists of $[FeS_5]$-trigonal bipyramids (tbp), which are linked by edges and corners into a $^2_\infty[Fe_2S_5]$-layer (Fig. 4). In this way, the 6+4 combination of coordination numbers in the polar chains is replaced by the 5+5 combination in the domain wall. In the other domain wall at $z \approx 0.6$, the $[FeS_4]$-tetrahedra of two opposing $^1_\infty[Fe_2S_5]$-chains share their vertices.

The sulfur anions eliminated thereby are counterbalanced by vacancies in the iron sites. Unlike the defect structure of $Ce_2Fe_{1.82}S_5$, the presence of vacancies does not entail the oxidation of other iron cations (instead less sulfur is incorporated). The apparent deficiency of FeS leads to the complicated sum formula $Ce_{22}Fe_{21}S_{54} = (11\ Ce_2Fe_2S_5–FeS)$.

The iron vacancies occur exclusively in octahedral chains and in the tbp domain wall. Remarkably, the occurrence of cation vacancies is not restricted to the spatial vicinity of the domain wall that contains the reduced amount of sulfur, but follows a sinusoidal occupation modulation through the entire structure (Fig. 3). The modulation of the positive charge can be approximated by a frozen charge-density wave with the wavelength $\lambda = c \sin\beta/2$ and the wavevector $k = 2\pi/\lambda = 4\pi c^*$.

To compensate for the cation vacancies in octahedral voids, the neighboring, originally tetrahedrally coordinated iron atoms in the same $^1_\infty[Fe_2S_5]$-chain shift in order to increase their coordination numbers towards [4+1]. The resulting coordination polyhedra have the shape of trigonal bipyramids. The fifth sulfur atom can be either part of the same $^1_\infty[Fe_2S_5]$-chain or part of a neighboring chain in the $^2_\infty[Fe_2S_5]$-layer (Fig. 5).

The Fe_{oct}–S bond lengths of 237–293 pm (Table 3) within the octahedra (oct) as well as the Fe–S distances of 224–303 pm within the distorted tetrahedra (tet, tbp) span a larger range than those in $Ce_2Fe_{1.82}S_5$ (220–253 pm) [6]. The coordination of the cerium atoms resembles that observed in $La_2Fe_2S_5$ quite closely [5], and is little affected by the defects in the $^1_\infty[Fe_2S_5]$-chains nor the distortions in the vicinity of the domain walls, except that some of the capping sulfur atoms are more distant. The Ce–S distances within the bicapped trigonal prisms are of 279–346 pm (Table 3), while those in $Ce_2Fe_{1.82}S_5$ are of 289–314 pm [6] and those in Ce_2SiS_5 are of 279–308 pm [14].

Inversion of the polarity of the $^1_\infty[Fe_2S_5]$-chains and thereby translation of the domain walls might be achieved by a shift of the iron atoms that reside in the tetrahedral sites. At a sufficiently high temperature, these cations should be able to switch to the opposite side of the octahedral chain, where they find again a tetrahedral coordination environment. Thus, a phase transition from the ferri- to the paraelectric state should take place, and the driving force of an external electrical field should be able to induce a preferred orientation of the moments.

The magnetic coupling within and between the $^1_\infty[Fe_2S_5]$-chains [8] strongly depends on the orientation of the capping tetrahedra. Consequently, any structural changes that are brought about by the application of an electrical field will also influence the magnetization of the compound. Hence, it will be worthwhile to explore the potential of $Ce_{22}Fe_{21}S_{54}$ for multiferroic applications, by extensive physical measurements.

Acknowledgments

We gratefully acknowledge the experimental help of Ms. J. Krug and the financial support of the Deutsche Forschungsgemeinschaft (DFG) within the Collaborative Research Center SFB 463.

References

[1] K. Mitchell, J.A. Ibers, Chem. Rev. 102 (2002) 1929.
[2] A.M. Mills, D. Bräunling, M. Ruck, Acta Crystallogr. C62 (2006) i56.

[3] (a) A.M. Mills, M. Ruck, Inorg. Chem. 45 (2006) 5172;
(b) D. Bräunling, S. Leoni, A.M. Mills, M. Ruck, Z. Anorg. Allg. Chem. 634 (2008) 107.
[4] (a) H. Schmid, Ferroelectrics (1994) 162–665;
(b) P. Murugavel, M.P. Singh, W. Prellier, B. Mercey, Ch. Simon, B. Raveau, J. Appl. Phys. 97 (2005), 103914/1–103914/4;
(c) Y. Furuya, M. Wuttig, I. Takeuchi, Kinzoku (2006) 76–367;
(d) Y. Furuya, I. Takeuchi, N. Imaizumi, Kinzoku (2006) 76–1303.
[5] (a) M. Patrie, H.D. Nguyen, J. Flahaut, C.R. Acad. Sci. Ser. C 266 (1968) 1575;
(b) G. Collin, P. Laruelle, Bull. Soc. Fr. Miner. Cristallogr. 94 (1971) 113;
(c) F. Besrest, G. Collin, J. Solid State Chem. 21 (1977) 161;
(d) F. Besrest, G. Collin, J. Solid State Chem. 24 (1978) 301.
[6] (a) A.M. Mills, W. Harms, M. Ruck, Z. Kristallogr. Suppl. 21 (2004) 173;
(b) W. Harms, A.M. Mills, T. Söhnel, C. Laubschat, F.E. Wagner, C. Geibel, Z. Hossain, M. Ruck, Solid State Sci. 7 (2005) 59.
[7] (a) G. Collin, F. Rouyer, J. Loriers, C.R. Acad. Sci. Ser. C266 (1968) 689;
(b) A.M. Mills, M. Ruck, Acta Crystallogr. C60 (2004) i71.
[8] (a) G. Collin, É. Barthélémy, O. Gorochov, C.R. Acad. Sci. Ser. C277 (1973) 775;
(b) R. Plumier, M. Sougi, G. Collin, Solid State Commun. 14 (1974) 971;
(c) R. Plumier, M. Sougi, M. Lecomte, J. Appl. Phys. 52 (1981) 2320;
(d) A. Schneidewind, A.M. Mills, W. Schnelle, O. Stockert, B. Ouladdiaf, M. Ruck, J. Magn. Magn. Mater. 310 (2007) 1706.
[9] H. von Wartenberg, Z. Anorg. Allg. Chem. (1956) 243–286.
[10] X-RED 1.22, Program for data reduction, STOE & Cie, Darmstadt, Germany, 2001.
[11] X-SHAPE 1.06, PROGRAM for crystal optimization for numerical absorption correction, STOE & Cie, Darmstadt, Germany, 1999.
[12] G.M. Sheldrick, Acta Crystallogr. A64 (2008) 112.
[13] K. Brandenburg, DIAMOND 3.1f, Crystal and Molecular Structure Visualization, Crystal Impact GbR, Bonn, Germany, 2008.
[14] G. Gauthier, S. Jobic, M. Evain, H.J. Koo, M.H. Whangbo, C. Fouassier, R. Brec, Chem. Mater. 15 (2003) 828.
[15] L. Barbour, LAYER, A programs to display diffraction data as precession photographs, Univ. of Missouri, Columbia, USA.